JOURNAL OF GEOPHYSICAL RESEARCH, VOL. 102, NO. A10, PAGES 22,261–22,272, OCTOBER 1, 1997

Proton transport model in the ionosphere 1. Multistream approach of the transport equations

M. Galand,[1] J. Lilensten, and W. Kofman

Centre d'Etudes des Phénomènes Aléatoires et Géophysiques, St Martin d'Hères, France

R.B.Sidje

Department of Mathematics, University of Queensland, Brisbane, Queensland, Australia

Abstract. The suprathermal particles, electrons and protons, coming from the magnetosphere and precipitating into the high-latitude atmosphere are an energy source of the Earth's ionosphere. They interact with ambient thermal gas through inelastic and elastic collisions. The physical quantities perturbed by these precipitations, such as the heating rate, the electron production rate, or the emission intensities, can be provided in solving the kinetic stationary Boltzmann equation. This equation yields particle fluxes as a function of altitude, energy, and pitch angle. While this equation has been solved through different ways for the electron transport and fully tested, the proton transport is more complicated. Because of charge-changing reactions, the latter is a set of two-coupled transport equations that must be solved: one for protons and the other for H atoms. We present here a new approach that solves the multistream proton/hydrogen transport equations encompassing the collision angular redistributions and the magnetic mirroring effect. In order to validate our model we discuss the energy conservation and we compare with another model under the same inputs and with rocket observations. The influence of the angular redistributions is discussed in a forthcoming paper.

1. Introduction

A few decades ago the theoretical analysis of the auroras was concerned mostly with the study of the electron precipitations. Indeed, electrons seemed to be the main source for the input energy needed to the excitation of the ambient neutrals at the origin of the northern lights. However, proton precipitations have been detected from ground observations [*Vegard*, 1948], and satellite or rocket measurements have corroborated their presence [*Sharp et al.*, 1967, 1969; *McNeal and Birely*, 1973, and references therein]. A statistical study [*Hardy et al.*, 1989] indicated that the integral energy flux of protons can equal or exceed that of the electrons for some latitudes and local times on the eveningside of the oval and that it is a significant fraction of the electron integral energy flux for much of the oval.

In response to these measurements, which tended to prove that protons were able to have a major influence on the polar ionosphere, the proton transport theory has received increased attention. To describe the energy loss undergone by the precipitating protons, studies by *Edgar et al.* [1973, 1975] assumed that the particles were slowed down continuously in the medium. By introducing an energy deposition function and setting a value for the energy loss per electron-ion pair, *Rees* [1982] determined several physical quantities, such as electron production or emission rates. *Jasperse and Basu* [1982] were the first to apply linear transport theory to proton-hydrogen aurora: Comparisons with incoherent scatter radar data showed that the electron density, an integrated quantity, agreed well with observations [*Basu et al.*, 1987; *Senior et al.*, 1987]. This first model derived closed-form analytic solutions. *Basu et al.* [1990] described a new, fully numerical model without the limiting approximation used in the earlier model. Moreover very recently a solution of transport equations in two spatial and three velocity dimensions was proposed by *Jasperse* [1997] to investigate the beam-spreading effect. The proton transport was also simulated by a Monte Carlo method and the collision-by-collision degradation scheme [*Kozelov and Ivanov*, 1992; *Kozelov*, 1993; *Kozelov and Ivanov*, 1994]. All these methods aim to describe the energetic degradation of the precipitating protons by interacting with ambient neutrals and the derived quantities, such as the electron production, the energy deposition function or the energy loss per electron-ion pair. Recently *Decker et al.* [1996] performed a comparison of three of these methods, a Monte Carlo simulation [*Kozelov and Ivanov*, 1992], a discrete energy loss solution to the linear transport equations [*Basu et al.*, 1993], and a continuous slowing down approximation [*Decker et al.*, 1996]. The agreement of the three models is excellent except at the lowest altitudes, largely below the region where the bulk of energy deposition and ionization takes place.

If today the purpose of a good description of energy degradation seems to have been reached, another problem remains unsolved. That deals with the origin of the red Doppler shift of H emissions. Historically, there are the Balmer H emissions observed from ground that allowed the detection of the proton precipitations [*Vegard*, 1939, 1948], and the first theoretical studies focused on these emissions [*Eather*, 1967,

[1]Now at High Altitude Observatory, National Center for Atmospheric Research, Boulder, Colorado.

Paper number 97JA01903.
0148-0227/97/97JA-01903$09.00

and references therein]. However the "red" Doppler shift of the H emissions on zenith profiles, defined as the extension of the profile at wavelenghts higher than the characteristic wavelength of the line, has not yet been surely explained: It attests to upward H atoms and thus proves that angular redistribution acts upon the proton beam. As the transport of protons and hydrogen atoms is coupled via charge-changing reactions, angular redistribution of hydrogen atoms can find its origin in collisions or in the effect of the nonuniformity of the magnetic field lines; but the role played by each of these two possible causes has not yet been evaluated. Indeed, experiments alone cannot give the solution. Modeling as well is needed to resolve this problem. And the best way to conduct such a study is to first determine the fluxes of protons and hydrogen atoms. Previous models based on the solution of the transport equations have always neglected the two types of angular redistributions [*Basu et al.*, 1993; *Decker et al.*, 1996]. No upward particle flux is then generated. Other models based on the Monte Carlo method have included angular redistributions sources and were applied to a monoenergetic beam in a N_2 atmosphere. Studies of the effects of these sources have been carried out for the collisional scattering on integrated quantities [*Kozelov and Ivanov*, 1992] and for the magnetic mirror force [*Kozelov*, 1993]. However the origin of the red shift has not yet been investigated with these models.

In the present study we solve the transport equations in a very general way that takes into account the collisional and magnetic mirroring angular redistributions. Moreover, no restrictions are applied on the incident proton beam or on the neutral model. We shall describe the way we have followed. The energy loss is assumed to be continuous which is justified a priori in section 2. The solution based on the introduction of dissipative forces is done in section 3. In the last section the model is validated, in the case of no angular redistribution, through a comparison with the model of *Basu et al.* [1993], whose results are presented by *Strickland et al.* [1993]. Another validation based on the evaluation of energy conservation is also presented. Finally, comparisons with the Proton I rocket data are shown [*Söraas et al.*, 1974]. The influence of the angular redistributions, especially the magnetic mirroring effect, is the subject of a forthcoming paper.

2. Continuous Energy Loss

Our solution makes a link between two approaches presented above: The continuous slowing down (CSD) approximation is applied to part of the collision operator in order to solve the two coupled transport equations. Under the CSD approximation the energetic particles, protons, and hydrogen atoms are assumed to be continuously degraded in energy in the medium. Such an approximation can be justified a priori if the energy losses W of the energetic particles are small compared to their energies E. In this section we ascertain this assumption by evaluating the relative energy loss W/E of protons and hydrogen atoms.

The ambient neutrals considered here are N_2, O_2, and O. The collision processes between an energetic particle, proton or H atom, and a neutral particle are the ionization or the excitation of the neutrals, the elastic scattering of the energetic particles, and the charge-changing reactions, that is, capture and stripping. For the inelastic processes, that is, for all those except the elastic scattering, the energy loss is provided by *Basu et al.* [1993]. The associated relative energy loss is plotted versus the energy of the protons or hydrogen atoms in Figure 1a. This loss is less than 2% above 1 keV. Therefore the CSD approximation is justified. This needs of course constant checking. That will be shown later in section 4.2 on through the computation of the energy conservation.

Unlike electrons, protons and hydrogen atoms, owing to their higher mass, can undergo a significant energy loss during elastic scattering. There is an interaction between the incident particle of mass m and a neutral target particle of mass m_α. The latter is assumed to be at rest because the thermal velocity is much smaller than the speed of the incoming energetic particles. As the type of the interaction between the two particles is elastic, it is possible to apply energy and momentum conservation. This yields the following form for the relative energy loss:

$$\frac{W}{E} = 1-\left(\frac{m}{m+m_\alpha}\right)^2 \cdot \left(\cos\varphi+\sqrt{\frac{m_\alpha^2}{m^2}-\sin^2\varphi}\right)^2 \quad (1)$$

where φ is the scattering angle of the energetic particle. The mass m, which refers to the proton or H mass, is equal to 1 g/mol, that is, $1.67\text{x}10^{-24}$ g; the mass m_α is equal to 14 g/mol, that is $2.34\text{x}10^{-23}$ g, for N and to 16 g/mol, that is, $2.67\text{x}10^{-23}$ g, for O.

The relative energy loss for elastic scattering is presented on Figure 1b. It is independent of the energy of the incident particle but depends on the scattering angle of this particle. Moreover, it can reach values higher than 20%. However, the most probable scattering angles are lower than 20° by far [*Fleischmann et al.*, 1967, 1974; *Newman et al.*, 1986; *Johnson et al.*, 1988; *Gao et al.*, 1990]; within this angle range, the relative energy loss does not exceed 1%. Therefore the CSD approximation is also a priori justified for this process.

Such an approximation has already been applied by *Edgar et al.* [1973, 1975]. The method they used is described by *Miller and Green* [1973]. It is based on the solution of the following equation:

$$L(E) = \frac{1}{n}\frac{dE}{dz} \quad (2)$$

where dE is the average energy loss over an incremental distance dz in a gas of density n.

The energy loss function L can be deduced from cross sections and energy losses associated to the different collision processes. However, owing to the charge-changing collisions, it involves the unknown proportion of the different charge states in the beam. Therefore they assumed that the beam is charge equilibrated; that is, the loss function for a given charge state is weighted by the relative equilibrium fraction. But at the top of the atmosphere, the beam is usually a pure proton beam and tends to be at equilibrium only as the beam penetrates into the atmosphere. In addition, although it is easy to integrate (2) when the medium is made of one constituent, there is no analytical solution in a multicomponent atmosphere, as in the Earth's atmosphere.

Recently an improved method was proposed by *Decker et al.* [1996] which uses a nonequilibrium flux. At each altitude level the charge state fractions are deduced from the transport equations by neglecting the energy loss. These fractions are used to determine the total energy loss functions; (2) is then solved to estimate the effects of energy degradation on the

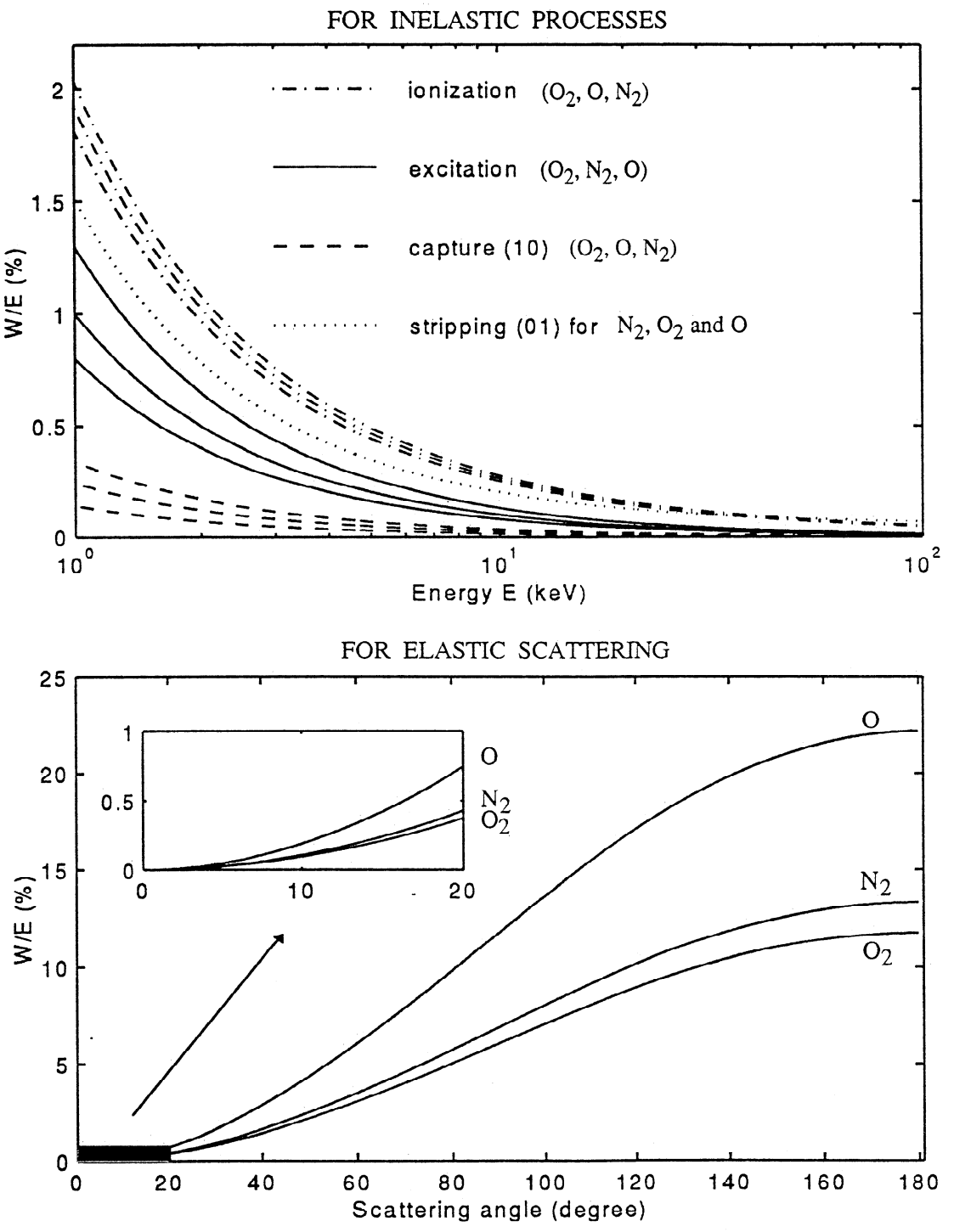

Figure 1. (a) Relative energy loss versus the energy of the proton or the H atom, for the inelastic processes. For each reaction the neutral species are specified in the order of the increasing values of the energy loss. For stripping, the energy loss is independent of the neutral species. (b) Relative energy loss versus the scattering angle of the proton or H atom. A detail is given at low angles, below 20°; that is, the most probable scattering range deduced from the data of differential cross sections.

incident proton beam. However, it is only the average energy loss for protons and H atoms together which is calculated, while the energy losses of charge-changing collisions are very different between protons and H atoms. Moreover, this method can be applied only to a monoenergetic and monodirectional streams, and it has to be assumed that the pitch angle of precipitating particles is constant as the particles penetrate down through the atmosphere. Therefore no angular redistribution can be included.

In the present study we apply the CSD approximation, that is the continuous degradation of precipitating particles in energy, and we introduce energy loss functions deduced from the cross sections and energy losses. But the analogy with the method of *Miller and Green* [1973] or the one proposed by

Decker et al. [1996] stops here. The loss functions we use are unique for each collision process between an energetic particle of a given charge state and a given neutral species without assumptions on the charge state proportion or without introducing an average energy loss. Moreover, the energy loss functions can depend on the angular redistribution. Finally, they are directly introduced in the general transport equation which describes the evolution of the flux of protons or of hydrogen atoms in altitude, in energy, and in pitch angle.

3. Solution of the Transport Equations

Our description of proton transport in the Earth's auroral region is based on the Boltzmann equation:

$$\frac{\partial f}{\partial t}(\mathbf{r},\mathbf{v},t)+\mathbf{v}.\nabla_{\mathbf{r}} f(\mathbf{r},\mathbf{v},t)+\nabla_{\mathbf{v}}\left(\frac{\mathbf{F}}{m} f(\mathbf{r},\mathbf{v},t)\right)=\left(\frac{\delta f}{\delta t}\right)_{\text{coll}} \quad (3)$$

where $\mathbf{r}$ and $\mathbf{v}$ are the position and the velocity vectors and the term on the right side in $cm^{-6}\ s^2$ is the usual source or sink term due to collisions with neutrals.

The unknown f is the distribution function of one particle in the six-dimensional phase space $(\mathbf{r},\mathbf{v})$. Its units are $cm^{-6}\ s^3$. This equation is the general transport equation, which is valid for a dissipative system. The originality of our solution lies in the fact that we have introduced dissipative forces to describe energetic degradation with neutrals usually taken into account in the collision term on the right side.

3.1 With the Forward-Scattering Approximation

In the first stage we assume that the particles are not redistributed in angle during a collision. The CSD approximation allows us to use a continuous function in energy to describe the energetic degradation of protons and H atoms; this function, L, is the loss function defined previously, in section 2. But here this function is relative to a process j (ionization, excitation, or charge-changing reactions) between a particle γ (proton or H atom) of energy E and a neutral α:

$$L^j_{\alpha,\gamma}(E)=W^j_{\alpha,\gamma}(E).\,\sigma^j_{\alpha,\gamma}(E) \quad (4)$$

where W and σ are the energy loss and the cross section, respectively.

By analogy with friction of energetic electrons on the thermal ambient electrons [*Stamnes and Rees*, 1983], it is then possible to introduce a dissipative force to consider the energy loss of the particle γ during the process j with the neutral species α:

$$\mathbf{F} = -n_\alpha(s).\,L^j_{\alpha,\gamma}(E).\,\frac{\mathbf{v}}{v} \quad (5)$$

where n_α is the density of species α and s the space variable taken along the magnetic field line.

Therefore, after the variable change from the distribution function f to the particle flux Φ, a measurable quantity, the transport equation (3) can be written as [*Stamnes and Rees*, 1983]

For protons (P):

$$\mu\frac{\partial}{\partial s}\left(\Phi_P(s,E,\mu)\right)+\mu\frac{d\mu}{ds}\frac{\partial}{\partial\mu}\left(\Phi_P(s,E,\mu)\right)$$

$$-\sum_\alpha\sum_{k=ioni,exci} n_\alpha(s)\frac{\partial}{\partial E}\left(L^k_{\alpha,P}(E).\,\Phi_P(s,E,\mu)\right)$$

$$-\sum_\alpha n_\alpha(s)\frac{\partial}{\partial E}\left(L^{01}_\alpha(E).\,\Phi_H(s,E,\mu)\right)$$

$$=-\sum_\alpha n_\alpha(s).\,\sigma^{10}_\alpha(E).\,\Phi_P(s,E,\mu)$$

$$+\sum_\alpha n_\alpha(s).\,\sigma^{01}_\alpha(E).\,\Phi_H(s,E,\mu) \quad (6a)$$

For H atoms (H):

$$\mu\frac{\partial}{\partial s}\left(\Phi_H(s,E,\mu)\right)$$

$$-\sum_\alpha\sum_{k=ioni,exci} n_\alpha(s)\frac{\partial}{\partial E}\left(L^k_{\alpha,H}(E).\,\Phi_H(s,E,\mu)\right)$$

$$-\sum_\alpha n_\alpha(s)\frac{\partial}{\partial E}\left(L^{10}_\alpha(E).\,\Phi_P(s,E,\mu)\right)$$

$$=-\sum_\alpha n_\alpha(s).\,\sigma^{01}_\alpha(E).\,\Phi_H(s,E,\mu)$$

$$+\sum_\alpha n_\alpha(s).\,\sigma^{10}_\alpha(E).\,\Phi_P(s,E,\mu) \quad (6b)$$

The units of the flux Φ are $cm^{-2}\ s^{-1}\ eV^{-1}\ sr^{-1}$. The variable μ is the cosine of the pitch angle, the angle between the magnetic field line and the velocity vector of the particle. It is negative for downward, positive for upward particles. The coupling of the two transport equations (6) is via the charge-changing reactions, that is, the capture, denoted by 10, and the stripping, denoted by 01.

The steady state situation is assumed: the collision frequencies being of about 1 to 100 s^{-1}, the characteristic time of these processes is largely smaller than the duration of stable proton precipitations ranging from several minutes to few hours. Electric fields are neglected. In velocity space the particle fluxes are assumed to possess azimuthal symmetry about the magnetic field lines. Thus the third term of (3) applied to the magnetic force in the proton equation becomes zero, as is shown in Appendix A. Moreover, the spreading of the beam, which is induced by the first path of the neutralized protons [*Iglesias and Vondrak*, 1974], is taken into account through an attenuation coefficient ε applied to the incident proton flux [*Jasperse and Basu*, 1982]. It is then possible to restrict ourselves to plane parallel geometry. The space variables reduce to one only, denoted by s, taken along the magnetic field line. This line is assumed to be a straight line. The region of interest is located between 80 and 800 km in the high-latitude region, where the variation of the dip angle does not exceed 0.8° and such an assumption is justified.

Protons are charged particles and undergo the magnetic mirroring effect. This is taken into consideration by the second term on the left side of (6a). Its form is discussed in a forthcoming paper. For hydrogen atoms this second term is assumed to be zero.

The process k is an ionization (ioni) or an excitation (exci). Since the forward-scattering approximation is assumed in section 3.1, the elastic scattering term is omitted. For a process k the energy redistribution of particles γ (P or H) is

considered through dissipative forces depending on the continuous loss functions L. Hence it appears in the left side and not in the right side, as in (3). The quantities describing the energy degradation can be put into two terms (see Appendix B, relation (B2), in the case of forward-scattering approximation):

$$-n_\alpha(s).\int_{>E}\sigma^k_{\alpha,\gamma}(E'\to E).\Phi_\gamma(s,E',\mu).\,dE'$$

$$+n_\alpha(s).\sigma^k_{\alpha,\gamma}(E).\Phi_\gamma(s,E,\mu)$$

The first illustrates the loss of particles γ of energy E' which leads to the production of particles γ of lower energy E. The second describes the loss of particles γ of energy E.

Unlike the process k leading to the production of a particle γ from a particle of the same charge state but of higher energy, a charge-changing reaction leads to the production or the loss of a particle of the other charge state: for these reactions, a part (at least) of the energetic degradation is present on the right side. Consider for example the case of the transport of the protons described by (6a). The capture 10 consists of the loss of protons of energy E. This is taken into account in the first term on the right side of (6a). The stripping 01 leads to the production of protons from H atoms of higher energy. This production can be considered thanks to a loss function applied to the H atom flux. It is included in the last term on the left side of (6a). Also, this term takes the loss of H atoms of energy E into account. Such a sink needs not be considered in the equation of protons: the second term on the right side of (6a) allows us to annihilate it. For H atom transport it is the same in switching P and H and in switching 01 and 10.

It should be noted that these productions or losses are artificial. There is not a particle which is absorbed and another which is produced. It is the same particle. However, such a separation is useful in the calculation of the gain or the sink of particles X of energy E and it does not affect the final result.

3.2 With Collisional Angular Redistribution

If we now consider the angular redistribution during a collision, a form more complete for the loss function has to be adopted:

$$L^j_{\alpha,\gamma}(E',\mu'\to\mu) = W^j_{\alpha,\gamma}(E',\mu'\to\mu).\sigma^j_{\alpha,\gamma}(E').\zeta^j_{\alpha,\gamma}(E',\mu'\to\mu) \quad (7)$$

where ζ represents the phase function illustrating the angular redistribution of the energetic particle γ, from the cosine of the pitch angle μ' to μ, during the process j with a neutral of species α. The process j can be an ionization, an excitation, an elastic scattering, or a charge-changing reaction.

So the coupled set of transport equations based on (6) takes the following shape:

$$\mu\frac{\partial}{\partial s}\left(\Phi_P(s,E,\mu)\right)+\mu\frac{d\mu}{ds}\frac{\partial}{\partial\mu}\left(\Phi_P(s,E,\mu)\right)$$

$$-\sum_\alpha n_\alpha(s).\sum_{k=ioni,exci,scat}\int d\mu'.\frac{\partial}{\partial E}\left(L^k_{\alpha,P}(E,\mu'\to\mu).\Phi_P(s,E,\mu')\right)$$

$$-\sum_\alpha n_\alpha(s).\int d\mu'.\frac{\partial}{\partial E}\left(L^{01}_\alpha(E,\mu'\to\mu).\Phi_H(s,E,\mu')\right)$$

$$=-\sum_\alpha n_\alpha(s).\sigma^T_{\alpha,P}(E).\Phi_P(s,E,\mu)+\sum_\alpha n_\alpha(s)$$

$$\times\sum_{k=ioni,exci,scat}\int d\mu'.\zeta^k_{\alpha,P}(E,\mu'\to\mu).\sigma^k_{\alpha,P}(E).\Phi_P(s,E,\mu')$$

$$+\sum_\alpha n_\alpha(s).\int d\mu'.\zeta^{01}_\alpha(E,\mu'\to\mu).\sigma^{01}_\alpha(E).\Phi_H(s,E,\mu') \quad (8a)$$

$$\mu\frac{\partial}{\partial s}\left(\Phi_H(s,E,\mu)\right)$$

$$-\sum_\alpha n_\alpha(s).\sum_{k=ioni,exci,scat}\int d\mu'.\frac{\partial}{\partial E}\left(L^k_{\alpha,H}(E,\mu'\to\mu).\Phi_H(s,E,\mu')\right)$$

$$-\sum_\alpha n_\alpha(s).\int d\mu'.\frac{\partial}{\partial E}\left(L^{10}_\alpha(E,\mu'\to\mu).\Phi_P(s,E,\mu')\right)$$

$$=-\sum_\alpha n_\alpha(s).\sigma^T_{\alpha,H}(E).\Phi_H(s,E,\mu)+\sum_\alpha n_\alpha(s)$$

$$\times\sum_{k=ioni,exci,scat}\int d\mu'.\zeta^k_{\alpha,H}(E,\mu'\to\mu).\sigma^k_{\alpha,H}(E).\Phi_H(s,E,\mu')$$

$$+\sum_\alpha n_\alpha(s).\int d\mu'.\zeta^{10}_\alpha(E,\mu'\to\mu).\sigma^{10}_\alpha(E).\Phi_P(s,E,\mu') \quad (8b)$$

Equation (8a) is for protons (P), and (8b) is for H atoms (H). The different considered reactions are ionization (ioni), excitation (exci), elastic scattering (scat), capture (10) and stripping (01). The total cross section σ^T gathers the three first ones and capture for protons and stripping for H atoms.

The energetic degradation of particles is considered on the left side of (8a) and (8b) through two terms depending on loss functions. Owing to the angular redistribution, these terms have to be integrated over the incident pitch angles μ'. On the right side the collision term is reduced to the pure elastic reactions for all processes (ionization, excitation, elastic scattering, capture, and stripping), the energy losses are included on the left side.

Under the CSD approximation (8a) and (8b) are completely equivalent to the classical form where energetic redistributions are considered in the collision term (right side) as discrete losses. This is demonstrated in Appendix B. But the new form of transport equations obtained here is more general, and it allows us to include magnetic and collisional angular redistributions without complicating the numerical solution too seriously.

3.3 Numerical Solution

To obtain proton and H atom fluxes, one must solve the set of transport equations, (8a) and (8b), numerically. This process is two-fold. First is the discretization with respect to energy and angle on a two-dimensional grid. Second is the determination of the solutions by integrating between two successive points along the altitude scale. The first stage approximates partial derivatives in energy and angle with finite-differences and it is not impeded by the introduction of dissipative forces. Indeed, after this first stage the proton transport system (8a) and (8b) reduces to the very malleable inhomogeneous linear system of first-order differential equations in s:

$$\frac{\partial}{\partial s}\Phi = \mathbf{A}.\Phi + \mathbf{B} \tag{9}$$

where the unknown Φ is either the downward or upward flux of protons and H atoms over the energy grid and the half-angle grid. The matrix **A** describes the interaction between particle fluxes belonging to the same half-angle grid, that is, either within the downward flux or within the upward flux. If no angular redistribution is considered, the matrix **A** models the energetic degradation undergone by protons or H atoms through collisions with neutrals. The vector **B**, referred to as the forcing term, is present only if angular redistributions are taken into account. It models the coupling between downward and upward fluxes. Assuming the neutral densities and the magnetic mirroring term constant within two consecutive levels of altitude, the elements of the matrix **A** and the vector **B** are constant within this altitude layer.

The second stage of the numerical process is the most computer-intensive part of the overall computation. It involves retrieving the vector Φ at each level of altitude. This entails the computation of many matrix exponentials and/or related matrix functions. Indeed, the analytic solution of (9) is

$$\Phi(s) = \exp\left((s-s_0).\mathbf{A}\right).(\Phi_{s_0} + \mathbf{A}^{-1}.\mathbf{B}) - \mathbf{A}^{-1}.\mathbf{B} \tag{10}$$

where Φ_{s_0} is the initial condition of the differential system. Note that the calculations are performed in two phases. First, from the top to the bottom of the atmosphere, for the downward flux. Next, from the bottom to the top, for the upward flux. For the downward flux, Φ_{s_0} is taken as the flux at the higher level of the altitude layer, while for the upward flux it is taken as the flux at the lower altitude level. When the forcing term **B** is zero, the differential system becomes homogeneous and the solution reduces to

$$\Phi(s) = \exp\left((s-s_0).\mathbf{A}\right).\Phi_{s_0} \tag{11}$$

Matrix exponentials have received considerable attention. Although the problem of computing a matrix exponential is easy to state, numerous difficulties spring up in practice. These difficulties are exacerbated by such circumstances as largeness, stiffness, and accuracy. The renowned survey of *Moler and Van Loan* [1978] gives a stimulating insight into the problems encountered. In our case the matrix is large and sparse. The exponential of a matrix is full even if the matrix is sparse. The size of **A** is $(nb_E.nb_\mu, nb_E.nb_\mu)$ where nb_E is the number of levels on the energy grid and nb_μ is the number of levels on the pitch angle grid. In common situations, nb_E is equal to 200 and nb_μ is equal to 20. Hence the order of the matrix **A** is the product $nb_E.nb_\mu \geq 4000$. A full storage of a double precision matrix that large would necessitate 122 MB. Moreover, the matrix **A**, modeling mainly energetic degradation, has negative eigenvalues with a high ratio between the highest and the smallest. Consequently, the differential system is stiff, and this imposes very small step sizes when (9) is directly integrated with a general-purpose differential solver. In addition, the norm of **A** increases significantly as the altitude decreases, and so the computation of the matrix exponential becomes very ill conditioned. As a result of these concomitant circumstances, most of the classical matrix exponential algorithms are either unsatisfactory or practically unusable in our context.

We shall now outline a successful approach that overcomes these difficulties. It relies upon the key observation that one is not really interested in the matrix exponential operator as such. Rather, one is interested in its action on an operand vector. With this guiding principle in mind, very efficient and versatile implementations addressing both the homogeneous and inhomogeneous cases have been described by *Sidje* [1994, 1997] in accordance with *Gallopoulos and Saad* [1992]. To begin with, a reformulation is done to avoid the matrix inverse appearing in (10). It can be shown that the explicit solution of (9) satisfies

$$\Phi(s+h) = h.\xi(h\mathbf{A}).(\mathbf{A}.\Phi(s)+\mathbf{B}) + \Phi(s) \tag{12}$$

where $$\xi(x) = (\exp(x)-1)/x = \sum_{k=0}^{\infty} x^k/(k+1)!.$$

Worthy of note is the fact that the matrix actually involved in the right-hand side becomes $h.\mathbf{A}$. Hence h can be selected small enough to cope with matrices of high norm arising at low altitudes. The quantity h is a step size, and it is selected automatically within the algorithm. This selection is done in conjunction with error estimations ensuring that the desired accuracy is achieved. In a nutshell, we employ a discrete subdivision $s_0 > s_1 > \cdots > s_{p+1} = s$ of $[s,s_0]$ for the downward fluxes and $s_0 < s_1 < \cdots < s_{p+1} = s$ of $[s_0,s]$ for the upward fluxes. If we let $h_k = s_{k+1} - s_k$, the solution is retrieved with the following step-by-step integration scheme:

$$\begin{cases} \Phi(s_0) = \Phi_{s_0} \\ \Phi(s_{k+1}) = \Phi(s_k + h_k) \end{cases}$$

$$= \begin{cases} \Phi(s_0) = \Phi_{s_0} \\ \Phi(s_{k+1}) = h_k\,\xi(h_k\mathbf{A}).(\mathbf{A}.\Phi(s_k)+\mathbf{B}) + \Phi(s_k) \end{cases} \tag{13}$$

It is clear that the crux of the problem is a matrix function operation of the form $\mathbf{W} = \xi(h.\mathbf{M}).\mathbf{V}$ which must be performed for several values of h and **V**. The vector **W** is approximated with a Krylov subspace projection technique. The keystone of this projection approach is to approximate **W** by an element of the Krylov subspace defined as $K_q = \text{span}\{\mathbf{V}, (h\mathbf{A}).\mathbf{V}, (h\mathbf{A})^2.\mathbf{V}, \ldots, (h\mathbf{A})^{q-1}.\mathbf{V}\}$ where q, the dimension of K_q, can be chosen considerably small (e.g., q = 10) compared to $nb_E.nb_\mu$, the order of **A**. The original large problem is converted into a weak form, that is a small similar problem of size (q,q), involving the restriction of the operator **A** onto the Krylov subspace. In this way it becomes possible to handle the weak form with classical methods, such as the irreducible Pade method used in this study. The interested reader may find more details by *Sidje* [1997].

A remarkable facet of this projection technique is that, on the whole, the matrix **A** interacts only via matrix-vector products. Hence the technique is a "matrix-free" technique. It is independent of the matrix data-storage, and it allows incorporating high-efficient matrix-vector products with respect to the structure, the sparsity pattern, and the features of the matrix. Our matrix has a special sparsity pattern. It is a sparse lower block-bidiagonal matrix. Each bloc is associated with a given level of energy and describes the half-angle grid (down/up) for both charge-states. It is lower block-diagonal because fluxes of energy E_i are only connected to fluxes of energy E_{i-1}. Greater performance can be achieved by holding the matrix into a compact format and designing a fine-tuned matrix multiplication routine tailored for this special structure.

When no angular redistributions are considered, (9) is solved at several altitude levels from the top to the bottom of

the atmosphere. The boundary condition is the downward flux at the adjacent higher-altitude level. At the starting level of altitude (the top of the atmosphere), the incident downward flux is assumed to be a pure proton beam, precipitating between 800 and 600 km. Observations indicate that the incident downward flux is isotropic and is often very close to being a Maxwellian [*Basu et al.*, 1987; *Strickland et al.*, 1993]. Its characteristic energy is between a few keV and several tens of keV; its typical energy flux ranges from 0.5 to 1 erg cm^{-2} s^{-1}. When angular redistributions are considered, upward fluxes are generated inducing back (and forth) computation in the simulated atmosphere.

A code based on this solution has been developed. Given the incident downward proton flux at the top of the atmosphere and a neutral model, it determines the proton and H atom fluxes on a grid of altitude, energy and pitch angle. In the next section 4, several validations are proposed using results provided by this code.

4. Validation

In order to validate our code, comparisons with another model as well as with observations are presented in this section. For the model comparison, we proceed under the same assumptions as those used in the reference model especially concerning the angular redistribution. Therefore the magnetic mirror effect is neglected, and the forward-scattering approximation is assumed for the discussion in section 4. All interest is focused on the energy degradation and on the validation of our model.

4.1 Comparison With Another Model

Different models based on the solution of the proton transport equations but without angular redistributions have been developed [*Jasperse and Basu*, 1982; *Basu et al.*, 1990, 1993]. The most recent results are those of *Strickland et al.* [1993] and were obtained from the model of *Basu et al.* [1993]. They are taken as reference in order to validate our code. In addition to the assumptions concerning the angular redistributions we consider the same inputs, that is, the same atmosphere model obtained from MSIS 86, the same set of cross sections [*Basu et al.*, 1987], and the same incident proton flux, that is a Maxwellian distribution of characteristic energy E_0 and of energy flux Q_0 equal to $1/\varepsilon$ erg cm^{-2} s^{-1}. Moreover, the inner parameters concerning the boundary values of the altitude and energy grids are taken similarly [*Strickland et al.*, 1993]: The top of the atmosphere is taken to be equal to 600 km, the bottom is taken to be equal to 90 km, and the energy grid ranges from 1 to 105 keV. Both altitude and energy grids are chosen unevenly spaced with 82 and 200 levels, respectively. The μ grid is chosen uniform with 20 levels.

For both models the fluxes of protons and H atoms integrated in angle are presented versus energy and for different altitude levels in Figure 2. The characteristic energy E_0 is equal to 8 keV. The two sets of results are very similar. Such a good agreement allows us to validate not only our code but also our solution model, at least above 1 keV. Indeed, the results of *Strickland et al.* [1993] were obtained from a model in which energy losses are considered as discrete: The energetic redistribution appears in the collision term, that is, in the right side of (3). Unlike this approach, our model assumes the continuous slowing down degradation of the particles: The energy redistributions are taken into consideration through dissipative forces. The fluxes are then obtained from two models based on totally different premises; their agreement allows us to validate our code but also and above all our model for energies above 1 keV.

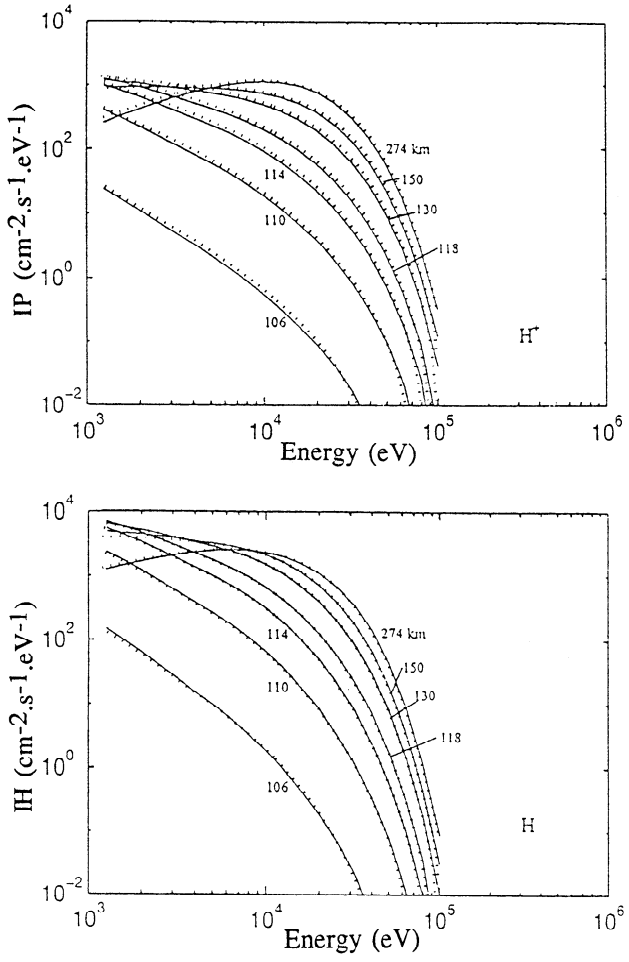

Figure 2. Comparison of proton fluxes (top) and H atom (bottom) as a function of energy, for different values of the altitudes. These fluxes are integrated in angle. The incident flux is assumed to be isotropic; it is given, in energy, by a Maxwellian distribution centered in 8 keV and with an energy flux equal to 1 erg cm^{-2} s^{-1}. The results provided by *Strickland et al.* [1993] are plotted in solid lines. Ours are shown with dotted curves. As we can see the two sets of results agree remarkably well.

A comparison of the electron production for three different values of the characteristic energy of the incident proton flux is presented on Figure 3. The electrons are produced by ionization of ambient neutrals or by stripping, that is, ionization of energetic H atoms:

$$Prion(s) = 2\pi \sum_{\alpha} n_{\alpha}(s).\int_{-1}^{0} d\mu.\int dE.\left\{\sigma_{\alpha,P}^{ioni}(E).\Phi_P(s,E,\mu) + \left(\sigma_{\alpha,H}^{ioni}(E)+\sigma_{\alpha}^{01}(E)\right).\Phi_H(s,E,\mu)\right\} \quad (14)$$

The higher the characteristic energy, the greater the depth of the atmosphere that the beam has to cross to be entirely

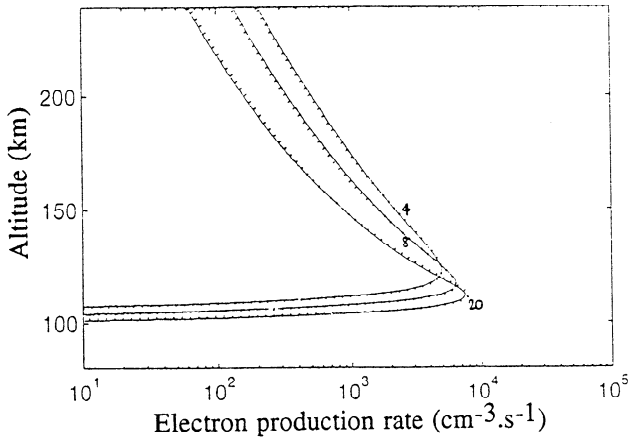

Figure 3. Comparison of electron production profiles in altitude, for incident fluxes given by isotropic 4-, 8-, and 20-keV Maxwellian distributions of energy flux equal to 1 erg cm^{-2} s^{-1}. The results provided by *Strickland et al.* [1993] are plotted in solid lines. Ours are shown with dotted curves. Here also, the two sets of results are in accordance.

degraded. In other words, the altitude of the production peak decreases as the energy E_0 increases.

Like the particle fluxes, the electron production profiles reported by *Strickland et al.* [1993] and those obtained from our model are very similar, which corroborates the validity of our model.

4.2 Energy Conservation

Another validation of our model lies in the check of the energy conservation. The incident energy flux Q_0 at the top of the atmosphere, weighted by the attenuation coefficient ε [*Basu et al.*, 1990], has to be equal to the total energy Q_e deposited in the atmosphere by energetic particles interacting with ambient neutrals. No particle exits the studied region. Since we neglect angular redistribution in the present section, no upward flux is generated and the lower altitude level is taken small enough to neglect the particle and energy fluxes below.

The energy deposition rate in eV cm^{-3} s^{-1} can be determined at a given altitude s by

$$\eta(s) = 2\pi \sum_{\alpha} n_\alpha(s).\iint \mathrm{d}\mu.\mathrm{d}\mu'.\int_0^\infty \mathrm{d}E' \times \sum_{\gamma=P,H} \sum_{j} L^j_{\alpha,\gamma}(E', \mu' \rightarrow \mu).\Phi_\gamma(s, E', \mu') \quad (15)$$

where j represents the ionization, excitation, elastic scattering, or charge-changing reactions.

Recall that the forward-scattering approximation is applied here, so that (15) can be simplified as

$$\eta(s) = 2\pi \sum_{\alpha} n_\alpha(s).\int \mathrm{d}\mu.\int_0^\infty \mathrm{d}E' \times \sum_{\gamma=P,H} \sum_{j} L^j_{\alpha,\gamma}(E').\Phi_\gamma(s, E', \mu) \quad (16)$$

It has to be underlined that although a loss function is introduced, no continuity assumption is made on the energetic degradation in relations (15) and (16). The same relations are used to determine the energy deposition rate when the discrete nature of the energy loss is under consideration in the model.

The energy grid ranges from a lower energy E_{min} to a higher energy E_{max}. The latter is chosen in such a way that the incident flux can be neglected above that threshold. However, the former is usually not equal to zero: the CSD approximation applied in our solution becomes invalid at low energies. Therefore the energy deposited at an energy lower than E_{min} is not included in (16). The associated energy deposition rate Q_{min} can be defined as the energy flux variation in altitude at E_{min}:

$$\frac{\partial}{\partial s} F(s, E_{min}) \qquad \text{where}$$

$$F(s, E_{min}) = 2\pi \int_{-1}^{0} |\mu|.\mathrm{d}\mu.E_{min}.\Delta E_{min}.\sum_{\gamma=P,H} \Phi_\gamma(s, E_{min}, \mu) \quad (17)$$

The pitch angle has negative values when it is relative to the downward flux.

The difficulty in (17) lies in the choice of the energy step ΔE_{min}. An overestimation of this step is obtained for $\Delta E_{min} = E_{min}$. So the energy E_{min} is chosen small enough to obtain a negligible value for Q_{min}. In practice, E_{min} is taken between 0.1 and 1 keV.

So with such appropriate choices for the energies E_{min} and E_{max}, the energy deposition rate $\eta(s)$ defined by (16) can be determined by

$$\eta(s) = 2\pi \sum_{\alpha} n_\alpha(s).\int \mathrm{d}\mu.\int_{E_{min}}^{E_{max}} \mathrm{d}E' \times \sum_{\gamma=P,H} \sum_{j} L^j_{\alpha,\gamma}(E').\Phi_\gamma(s, E', \mu) \quad (18)$$

The total energy deposition rate Q_e in the atmosphere (eV cm^{-2} s^{-1}) is defined by

$$Q_e = \int_{z_{min}}^{z_{max}} \eta(s).\mathrm{d}s \quad (19)$$

where z_{min} and z_{max} are the lowest and highest altitude levels, respectively.

The check of the conservation of energy reduces to showing that the incident energy flux $\varepsilon.Q_0$ and the total energy deposition rate Q_e are equal. As Q_e is proportional to ε, the energy conservation check does not depend on the attenuation coefficient. Taking a sufficient number of levels on the altitude, energy and angle grids, the solutions of the transport equations fulfill the energy conservation with a margin of a discrepancy less than 3%. Furthermore, this validation shows that the CSD approximation is valid even for relatively low energies, of a few hundreds of eV.

It has to be noted that the energy conservation applied here is based on physical considerations: The energy deposition rate depends on cross sections and loss functions for the different collisional processes. *Basu et al.* [1990] propose another form to evaluate the energy deposition rate:

$$\eta_B(s) = -2\pi \int_{-1}^{0} \mu.\mathrm{d}\mu.\int_{E_{min}}^{E_{max}} E.\mathrm{d}E.\frac{\partial}{\partial s} \sum_{\gamma=P,H} \Phi_\gamma(s, E, \mu) \quad (20)$$

This relation enables us to estimate the energy deposition directly from the flux: The energy deposited at each altitude layer is equal to the difference of the inward and the outward energy fluxes. This energy conservation check tests merely the numerical integration scheme, however, and provides a much weaker test than using (18) and (19) to compare with the incident energy flux.

By comparing with another model and by checking the conservation of energy, the proton transport code has been validated theoretically. At this step of the study a comparison of the proton code with observations seems now to be essential.

4.3 Comparison With Observations

The majority of physical quantities perturbed during proton precipitations, such as electron density and emission intensities, can be determined from particle fluxes. Therefore the most effective comparison with observations deals with proton and H atom fluxes. We present modeled fluxes to compare to proton and H atom flux data measured aboard a rocket.

The vehicle Proton I was launched from Andöya, Norway, located at 69°18'N and 16°01'E. The flight occurred on February 13, 1972, at 0024 LT during little perturbed conditions: the magnetic index Ap was 22 and the Sun index $f_{10.7}$ was 126.3. The rocket reached an altitude of 224 km. During the flight, proton and H atom fluxes were measured at different altitude levels and for different energy and pitch angle ranges. The data used here concern particles of high energy greater than 30 keV. Measurements were done at lower energies thanks to another detector, but the uncertainties on these data are relatively high (F.Söraas, personal communication, 1996). A more comprehensive description of the flight, the pay load, and the measurements is provided in *Söraas et al.* [1974, 1994].

The flight lasted almost 7 min, during which the Hβ emission measured from ground decreased slowly. The rocket was launched almost perpendicular to the magnetic field lines (azimuth of 340°). However, the aurora appeared as a nearly homogeneous glow despite some faint additional structures, and no marked variations occurred during the flight: in first approximation the precipitation can be assumed to be spatially stable and temporally constant, at least during the ascent or the descent part of the flight.

Under these assumptions it is possible to deduce the incident flux from a measurement at apogee. At apogee the vehicle was at an altitude of 224 km and the proton beam had not yet undergone significant energy losses, at least above 1 keV. The proton beam at this altitude is at charge equilibrium. Therefore the proton flux incident at an altitude of 800 km upon the ionosphere is taken to be equal to the flux of protons and H atoms measured at 224 km for energies greater than 30 keV. From *Söraas el al.* [1974] this downward flux can be assumed to be isotropic and its distribution in energy can be approximated by the following functions:

$$\Phi(E) = 8 \times 10^7 E^{-2} \quad \text{with } 1 < E < 100 \text{ keV} \quad (21a)$$

$$\Phi(E) = 2.2 \times 10^{17} E^{-6.67} \quad \text{with } E > 100 \text{ keV} \quad (21b)$$

with the particle energy E in keV and the particle flux Φ in $cm^{-2}\ s^{-1}\ keV^{-1}\ sr^{-1}$.

Nevertheless we should point out that the flux which has truly precipitated at 800 km must have been higher. Indeed, at high altitude the incident proton beam is spread by the first path of the neutralized protons. This leads to an attenuation of the particle flux at the center of the beam [*Iglesias and Vondrak*, 1974]. In the proton code this attenuation is neglected since it is already taken into account when using the measured flux as a boundary condition for the incident flux at the top of the atmosphere.

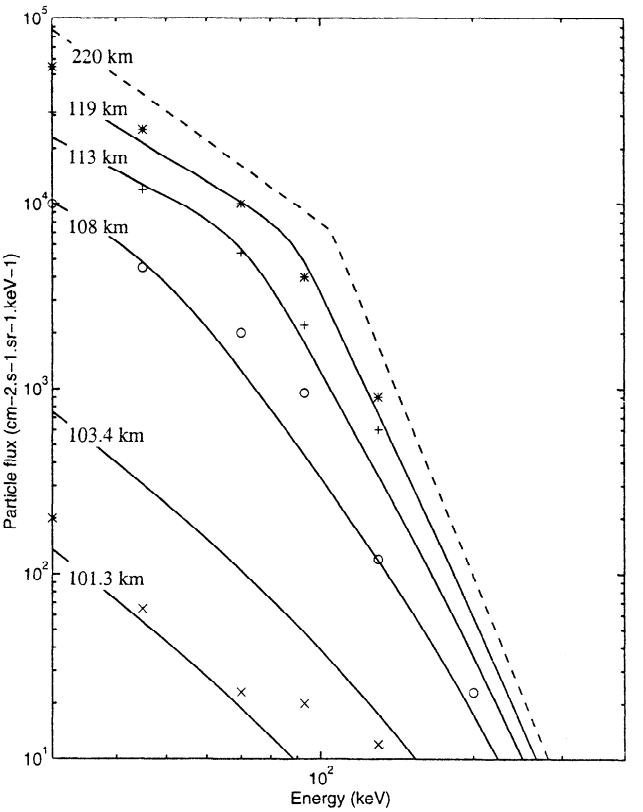

Figure 4. Comparison of energetic distributions of (H^++H) fluxes at different altitudes. Proton I rocket data [*Söraas et al.*, 1974] are represented with symbols and are valid for pitch angles between 152 and 165°. The asterisks, pluses, circles, and crosses refer to the altitude ranges 118.4-119.9 km, 112.8-114.2 km, 108.5-109.9 km and 102.5-104.0 km, respectively. The results obtained from the transport code are illustrated with solid lines and the altitudes associated are directly given on the figure. The incident flux taken equal to the measured flux at 220 km [*Söraas et al.*, 1974] is plotted with the dashed line.

We use the proton code to compare the predicted fluxes at lower altitudes with Proton I rocket data. The neutral model from 90 to 800 km is deduced from MSIS 90 for the day of the experiment. The cross-section set is from *Basu et al.* [1987]. The incident proton flux is defined by (21a) and (21b). The energy grid spreads from 30 to 600 keV, following the energy range of proton and H atom data. The incident particle flux is negligible for energies greater than 600 keV. It should be emphasized that incident particles of energies lower than 30 keV have no effect on the present results because the energy degradation is from higher to lower energies.

Particle Flux as a Function of Energy. The particle flux data obtained during the ascending part of the flight are represented versus energy with stars on Figure 4 for different altitude levels. The fluxes provided by the proton transport code are plotted in solid lines on Figure 4, too. There is good agreement between measured and calculated results presented in Figure 4. The small differences can be explained by the uncertainties in the data as well as in the input parameters. The observed particle fluxes are known with an uncertainty of 20% and the cross sections with an uncertainty of 30%. Moreover, the stability assumed in time

and in space of the incident flux is only an approximation: This represents another possible source for the discrepancy, but it is difficult to evaluate.

The most noticeable disagreement appears at low altitude. The measured flux between 102.5 and 104 km is framed by the calculated fluxes at 101.3 and 103.4 km. This altitude region is located below the energy deposition altitude at about 110 km: The particle flux decreases very fast since the neutral density is high. We checked that the uncertainty on the neutral model as well as on the measured altitude known to an accuracy of 1 km can easily explain the discrepancy.

For an incident flux based on observations at 224 km and for energies higher than 30 keV, the agreement between measured and calculated energy distributions of particle fluxes is rather good. In spite of all the uncertainties already pointed out, this comparison is a first step toward a satisfying validation of the modeled energetic degradation, at least above 30 keV, in our proton transport code. For further validation we need more rocket observations. At the present, to our knowledge, only this experiment fits the requirements for such a comparison.

5. Conclusion

The solution of transport equations allows the most complete study of the interaction of a proton beam with the atmosphere. The approach described here includes processes neglected until now, such as angular redistribution due to collisional interaction as well as magnetic mirroring. The red shift on Doppler profiles of H emissions attests of upward flux generated from proton precipitation.

In section 2, the study of energy losses of protons and H atoms has led to assume that these particles are slowed down in the atmosphere continuously. Therefore it has been possible to introduce dissipative forces depending on cross sections and energy losses to describe the energy degradation due to collisions with neutrals. The solution is then based on the general transport equation instead of on a restricted equation valid only for conservative forces and used until now in the literature of proton transport. Our solution allows the introduction of angular redistribution without seriously complicating the solution.

A code has been developed based on this approach. The results obtained were compared with those from another model [*Basu et al.*, 1993; *Strickland et al.*, 1993]. For consistency we considered the same assumptions used in this model, especially no angular redistributions. Basu's code is based on another solution taking into account the discrete nature of the collision energy losses. Unlike them, our solution used the CSD approximation. Therefore the very good agreement between both models on the particle fluxes and electron production leads not only to the validation of our code but also justifies the CSD approximation for energies above 1 keV.

Another validation based on physical consideration concerning the energy conservation is discussed. Energy loss in the code is less than 3% and allows us to show that the CSD approximation is still accurate down to a few hundreds of eV.

A comparison with Proton I rocket data based on energy distribution of particle fluxes validated the energetic degradation and the continuous slowing down approximation at high energies above 30 keV.

In the present paper the solution of our model has been presented and the validation of our solution, especially the energetic degradation, has been discussed on theoretical as well as on experimental backgrounds. It now appears interesting to study the influence of angular redistribution sources whose effects have been underlined by ground-based observations of H emission Doppler profiles. The collisional angular redistributions could be important at low energies, mainly below 1 keV, and the magnetic mirroring effect could have a significant influence at high altitudes. However, ground-based observations cannot allow to identify the processes acting predominently on the proton beam. Since our code can include these sources, a theoretical analysis can be undertaken to study the effects of these processes on particle fluxes and their influence on the Doppler profile of H emissions. These results are the subject of a forthcoming paper.

Appendix A: The Magnetic Force

If the third term of (3) is applied to the Lorentz force, it takes the following form:

$$\frac{1}{m}\nabla_{\mathbf{v}}\left((q\,\mathbf{v}\wedge\mathbf{B}).\,f(\mathbf{r},\mathbf{v},t)\right) = \frac{q}{m}f(\mathbf{r},\mathbf{v},t).\,\nabla_{\mathbf{v}}(\mathbf{v}\wedge\mathbf{B}) + \frac{q}{m}(\mathbf{v}\wedge\mathbf{B}).\,\nabla_{\mathbf{v}}\left(f(\mathbf{r},\mathbf{v},t)\right) \qquad \text{(A1)}$$

As the magnetic force is not dissipative, the first term of (A1) is equal to zero.

As for the second term of (A1), it can be rewritten (A2)

$$\frac{q}{m}v^2.f(\mathbf{r},\mathbf{v},t).(\mathbf{v}\wedge\mathbf{B}).\nabla_{\mathbf{v}}\left(\frac{1}{v^2}\right)+\frac{q}{v^2}(\mathbf{v}\wedge\mathbf{B}).\,\nabla_{\mathbf{v}}\left(\frac{v^2}{m}f(\mathbf{r},\mathbf{v},t)\right)$$

But,

$$\Delta\,\nabla_{\mathbf{v}}\left(\frac{1}{v^2}\right) = \sum_{i=1}^{3}\mathbf{e_i}\cdot\frac{\partial}{\partial v_i}\left(\frac{1}{v^2}\right) = -\frac{2\mathbf{v}}{v^4} \qquad \text{with } \mathbf{v}=\sum_{i=1}^{3}v_i.\,\mathbf{e_i}$$

Then, as the Lorentz force is perpendicular to the vector $\mathbf{v}$, the first term of (A2) is equal to zero.

Δ by the definition and the characteristics of the particle flux Φ [*Stamnes and Rees*, 1983],

$$\nabla_{\mathbf{v}}\left(\frac{v^2}{m}f(\mathbf{r},\mathbf{v},t)\right) = \nabla_{\mathbf{v}}\left(\Phi(s,E,\mu)\right) \qquad \text{with } \mu=\frac{v_3}{v}=u_3$$

and

$$\nabla_{\mathbf{v}} = \sum_{i=1}^{3}\mathbf{e_i}\cdot\frac{\partial}{\partial v_i} = \sum_{i=1}^{3}\mathbf{e_i}\cdot\frac{\partial E}{\partial v_i}\frac{\partial}{\partial E} + \sum_{i,j=1}^{3}\mathbf{e_i}\cdot\frac{\partial u_j}{\partial v_i}\frac{\partial}{\partial u_j} \qquad \text{with } \mathbf{u}=\frac{\mathbf{v}}{v}$$

$$= m\mathbf{v}\frac{\partial}{\partial E} - \sum_{j=1}^{3}\mathbf{v}.\frac{v_j}{v^3}\frac{\partial}{\partial u_j} + \sum_{j=1}^{3}\mathbf{e_j}\cdot\frac{1}{v}\frac{\partial}{\partial u_j}$$

Therefore the second term of (A2) takes the following form:

$$\frac{q}{v^2}(\mathbf{v}\wedge\mathbf{B}).\,\mathbf{v}.\left(m\frac{\partial}{\partial E}-\sum_{j=1}^{3}\frac{v_j}{v^3}\frac{\partial}{\partial u_j}\right).\Phi(s,E,\mu)$$

$$+\frac{q}{v^2}(\mathbf{v}\wedge\mathbf{B})\sum_{j=1}^{3}\mathbf{e}_j.\frac{1}{v}\frac{\partial}{\partial u_j}\Phi(s,E,\mu)$$

$$=\frac{q}{v^2}(\mathbf{v}\wedge\mathbf{B}).\mathbf{e}_3.\frac{1}{v}\frac{\partial}{\partial\mu}\Phi(s,E,\mu)\qquad\text{with }\mathbf{e}_3\text{ parallel to }\mathbf{B}$$

$$=\qquad 0$$

Appendix B: From the Continuous Energy Loss to the Discrete Energy Loss in the Transport Equation

In the set of transport equations (8a) and (8b), the energy degradation undergone by precipitating particles γ (P or H) during a collision j with a neutral species α is

$$-n_\alpha(s)\frac{\partial}{\partial E}\left(\int_{-1}^{1}L^j_{\alpha,\gamma}(E,\mu'\to\mu).\Phi_\gamma(s,E,\mu').\,d\mu'\right)$$

$$=-n_\alpha(s)\int_{-1}^{1}\frac{\partial}{\partial E}\left(L^j_{\alpha,\gamma}(E,\mu'\to\mu).\Phi_\gamma(s,E,\mu').\,d\mu'\right)$$

(because the function $L^j_{\alpha,\gamma}.\Phi_\gamma$ is continuous on its definition domain and has a partial derivative in μ' continuous on this same set)

$$\approx-n_\alpha(s)\int_{-1}^{1}\left(\frac{L^j_{\alpha,\gamma}(E+W,\mu'\to\mu).\Phi(s,E+W,\mu')}{W}-\frac{L^j_{\alpha,\gamma}(E,\mu'\to\mu).\Phi_\gamma(s,E,\mu')}{W}\right).d\mu'$$

(because the energy degradation is assumed to be continuous (CSD approximation): $W\langle\langle E$, with $W=W^j_{\alpha,\gamma}$, the energy loss undergone by the particle γ)

$$=-n_\alpha(s)\times\int_{-1}^{1}\sigma^j_{\alpha,\gamma}(E+W).\zeta^j_{\alpha,\gamma}(E+W,\mu'\to\mu).\Phi_\gamma(s,E+W,\mu').\,d\mu'$$

$$+n_\alpha(s).\int_{-1}^{1}\sigma^j_{\alpha,\gamma}(E).\zeta^j_{\alpha,\gamma}(E,\mu'\to\mu).\Phi_\gamma(s,E,\mu').\,d\mu'$$

(from the definition relation (7) of L, and in assuming that the energy loss varies slowly versus the energy of the particle: $W = w(E,\mu'\to\mu)\approx w(E+W,\mu'\to\mu)$. This is checked by the low and continuous variation of the relative energy loss plotted on Figure 1)

The following relation introduces the differential cross-section

$$\sigma^j_{\alpha,\gamma}(E',\mu'\to E,\mu)=\sigma^j_{\alpha,\gamma}(E').\delta\left(E',E+W^j_{\alpha,\gamma}\right).\zeta^j_{\alpha,\gamma}(E',\mu'\to\mu)\qquad\text{(B1)}$$

with δ, the dirac function. The energy degradation term in (8a) and (8b) can then be rewritten as

$$-n_\alpha(s)\frac{\partial}{\partial E}\left(\int_{-1}^{1}L^j_{\alpha,\gamma}(E,\mu'\to\mu).\Phi_\gamma(s,E,\mu').\,d\mu'\right)$$

$$=-n_\alpha(s)\times\int_{>E}\int_{-1}^{1}\sigma^j_{\alpha,\gamma}(E',\mu'\to E,\mu).\Phi_\gamma(s,E',\mu').\,dE'.\,d\mu'$$

$$+n_\alpha(s).\sigma^j_{\alpha,\gamma}(E)\int_{-1}^{1}\zeta^j_{\alpha,\gamma}(E,\mu'\to\mu).\Phi_\gamma(s,E,\mu').\,d\mu'\qquad\text{(B2)}$$

The first term on the right side of (B2) describes the production of particles of type (E,μ) from particles γ of type (E',μ') of higher energy. The second term is equal to the second term (or the third) on the right side of (8a) and (8b). Therefore the loss term of particles γ of type (E,μ) is the only term which does not disappear in the right side of (8a) and (8b). Finally, the transport equations (8a) and (8b) on which is based our proton transport code can be rewritten as follows:

$$\mu\frac{\partial}{\partial s}\left(\Phi_P(s,E,\mu)\right)+\mu\frac{d\mu}{ds}\frac{\partial}{\partial\mu}\left(\Phi_P(s,E,\mu)\right)$$

$$=-\sum_\alpha n_\alpha(s).\sigma^T_{\alpha,P}(E).\Phi_P(s,E,\mu)$$

$$+\sum_\alpha\sum_{k=exci,ioni,scat}n_\alpha(s)\times\int_{>E}\int_{-1}^{1}\sigma^k_{\alpha,P}(E',\mu'\to E,\mu).\Phi_P(s,E',\mu').\,dE'.\,d\mu'$$

$$+\sum_\alpha n_\alpha(s)\times\int_{>E}\int_{-1}^{1}\sigma^{01}_\alpha(E',\mu'\to E,\mu).\Phi_H(s,E',\mu').\,dE'.\,d\mu'\qquad\text{(B3a)}$$

$$\mu\frac{\partial}{\partial s}\left(\Phi_H(s,E,\mu)\right)$$

$$=-\sum_\alpha n_\alpha(s).\sigma^T_{\alpha,H}(E).\Phi_H(s,E,\mu)$$

$$+\sum_\alpha\sum_{k=exci,ioni,scat}n_\alpha(s)\times\int_{>E}\int_{-1}^{1}\sigma^k_{\alpha,H}(E',\mu'\to E,\mu).\Phi_H(s,E',\mu').\,dE'.\,d\mu'$$

$$+\sum_\alpha n_\alpha(s)\times\int_{>E}\int_{-1}^{1}\sigma^{10}_\alpha(E',\mu'\to E,\mu).\Phi_P(s,E',\mu').\,dE'.\,d\mu'\qquad\text{(B3b)}$$

Equations (B3a) and (B3b) represent the classical conservative transport equation used in all the proton transport solution so far [*Jasperse and Basu*, 1982; *Basu et al.*, 1990, 1993].

Acknowledgments. We would like to thank A. Richmond and P.-L. Blelly for really helpful discussions, as well as D. Lummerzheim for his enriching comments. We are indebted to B. Basu for providing us with input parameters in the view of the comparison with his model and to F. Söraas for useful comments on Proton I data. Part of the computations presented in this paper were performed at the Centre de

Calcul Intensif de l'Observatoire de Grenoble. Finally I would like to thank HAO/NCAR for supporting me during the writing of this article.

The Editor thanks R. Link and D. Lummerzheim for their assistance in evaluating this paper.

References

Basu, B., J. R. Jasperse, R. M. Robinson, R. R. Vondrak and D. S. Evans, Linear transport theory of auroral proton precipitation: a comparison with observations, *J. Geophys. Res.*, *92*, 5920, 1987.

Basu, B., J. R. Jasperse, and N. J. Grossbard, A numerical solution of the coupled proton-H atom transport equations for the proton aurora, *J. Geophys. Res.*, *95*, 19,069, 1990.

Basu, B., J. R. Jasperse, D. J. Strickland, and R. E. Daniell, Transport-theoretic model for the electron-proton-hydrogen atom aurora, 1, Theory, *J. Geophys. Res.*, *98*, 21,517, 1993.

Decker, D. T., B. V. Kozelov, B. Basu, J. R. Jasperse, and V. E. Ivanov, Collisional degradation of the proton-H atom fluxes in the atmosphere: A comparison of theoretical techniques, *J. Geophys. Res.*, *101*, 26,947, 1996.

Eather, R. H., Auroral proton precipitation and hydrogen emissions, *Rev. Geophys.*, *5*, 207, 1967.

Edgar, B. C., W. T. Miles, and A. E. S. Green, Energy deposition of protons in molecular nitrogen and applications to proton auroral phenomena, *J. Geophys. Res.*, *78*, 6595, 1973.

Edgar, B. C., H. S. Porter, and A. E. S. Green, Proton energy deposition in molecular and atomic oxygen and applications to the polar cap, *Planet. Space Sci.*, *23*, 787, 1975.

Fleischmann, H. H., R. A. Young, and J. W. McGowan, Differential charge-transfer cross section for collisions of H^+ on O_2, *Phys. Rev.*, *153*, 19, 1967.

Fleischmann, H. H., C. F. Barnett, and J. A. Ray, Small-angle scattering in stripping collisions of hydrogen atoms having energies of 1-10 keV in various gases, *Phys. Rev. A*, *10*, 569, 1974.

Gallopoulos, E., and Y. Saad, Efficient solution of parabolic equations by Krylov approximation methods, *SIAM J. Sci. Stat. Comput.*, *13*, 1236, 1992.

Gao, R. S., L. K. Johnson, C. L. Hakes, K. A. Smith, and R. F. Stebbings, Collisions of kilo-electron-volt H^+ and He^+ with molecules at small angles: Absolute differential cross sections for charge transfer, *Phys. Rev. A*, *41*, 5929, 1990.

Hardy, D. A., M. S. Gussenhoven, and D. Brautigam, A statistical model of auroral ion precipitation, *J. Geophys. Res.*, *94*, 370, 1989.

Iglesias, G. E., and R. R. Vondrak, Atmospheric spreading of protons in auroral arcs, *J. Geophys. Res.*, *79*, 280, 1974.

Jasperse, J. R., and B. Basu, Transport theoretic solutions for auroral proton and H atom fluxes and related quantities, *J. Geophys. Res.*, *87*, 811, 1982.

Johnson, L. K., R. S. Gao, K. A. Smith, and R. F. Stebbings, Absolute differential cross sections for very-small angle scattering of keV H and He atoms by H_2 and N_2, *Phys. Rev. A*, *38*, 2794, 1988.

Kozelov, B. V., Influence of the dipolar magnetic field on transport of proton-H atom fluxes in the atmosphere, *Ann. Geophys.*, *11*, 697, 1993.

Kozelov, B. V., and V. E. Ivanov, Monte Carlo calculations of proton-hydrogen atom transport in N_2, *Planet. Space Sci.*, *40*, 1503, 1992.

Kozelov, B. V., and V. E. Ivanov, Effective energy loss per electron-ion pair in proton aurora, *Ann. Geophys.*, *12*, 1071, 1994.

McNeal, R. J., and J. H. Birely, Laboratory studies of collisions of energetic H^+ and hydrogen with atmospheric constituents, *Rev. Geophys.*, *11*, 633, 1973.

Miller, J. H., and A. E. S. Green, Proton energy degradation in water vapor, *Radiat. Resear.*, *54*, 343, 1973.

Moler, C. B., and C. F. Van Loan, Nineteen dubious ways to compute the exponential of a matrix, *SIAM Rev.*, *20*, 801, 1978.

Newman, J. H., Y. S. Chen, K. A. Smith, and R. F. Stebbings, Differential cross sections for scattering of 0.5-, 1.5-, and 5.0-keV hydrogen atoms by He, H_2, and O_2, *J. Geophys. Res.*, *91*, 8947, 1986.

Rees, M. H., On the interaction of auroral protons with the earth's atmosphere, *Planet. Space Sci.*, *30*, 463, 1982.

Senior, C., J. R. Sharber, O. de la Beaujardière, R. A. Heelis, D. S. Evans, J. D. Winningham, M. Sugiura, and W. R. Hoegy, *E* and *F* region study of the evening sector auroral oval: A Chatanika/Dynamics Explorer 2/NOAA 6 comparison, *J. Geophys. Res.*, *92*, 2477, 1987.

Sharp, R. D., R. G. Johnson, M. F. Shea, and G. B. Shook, Satellite measurements of precipitating protons in the auroral zone, *J. Geophys. Res.*, *72*, 227, 1967.

Sharp, R. D., D. L. Carr, and R. G. Johnson, Satellite observations of the average properties of auroral particle precipitations: latitudinal variations, *J. Geophys. Res.*, *74*, 4618, 1969.

Sidje, R. B., Parallel algorithms for large sparse matrix exponentials, Ph.D. thesis, Univ. de Rennes 1, Rennes, France, 1994.

Sidje, R. B., EXPOKIT, Software package for computing matrix exponentials, ACM Trans. Math. Software, in press, 1997.

Söraas, F., H. R. Lindalen, K. Måseide, A. Egeland, T. A. Sten, and D. S. Evans, Proton precipitation and the Hβ emission in a postbreakup auroral glow, *J. Geophys. Res.*, *79*, 1851, 1974.

Söraas, F., K. Måseide, P. Torheim, and K. Aarsnes, Doppler-shifted auroral Hb emission: A comparison between observations and calculations, *Ann. Geophys.*, *12*, 1052, 1994.

Stamnes, K., and M. H. Rees, Inelastic scattering effects on photoelectron spectra and ionospheric electron temperature, *J. Geophys. Res.*, *88*, 6301, 1983.

Strickland, D. J., R. E. Daniell, J. R. Jasperse, and B. Basu, Transport-theoretic model for the electron-proton-hydrogen atom aurora, 2, Model results, *J. Geophys. Res.*, *98*, 21,533, 1993.

Vegard, L., Hydrogen showers in the auroral region, *Nature*, *144*, 1089, 1939.

Vegard, L., Emission spectra of night sky and aurora, Reports of the Gassiot Committee, *Phys. Soc. London*, *82*, 1948.

M.Galand, J, Lilensten, and W. Kofman, Centre des Phénomènes Aléatoires et Géophysiques, UPRESA 5083, BP 46, 38402 St Martin d'Hères, Cedex, France.

R.B. Sidje, Department of Mathematics, University of Queensland, Brisbane QLD 072, Australia.

Jasperse, J.R., Transport theoretic solutions for the beam-spreading effect in the proton-hydrogen aurora, *Geohys. Res. Lett.*, *24*, 1415, 1997.

(Received January 22, 1997; revised May 28, 1997;
accepted July 1, 1997.)